FIB TOMOGRAPHY OF WARK-LOVERING RIMS IN THE ALLENDE METEORITE J. Weber[1*], T. Ramprasad[1], K. Domanik[1], T. J. Zega[1] [1]Lunar and Planetary Laboratory, University of Arizona, USA. *julianeweber@email.arizona.edu

Introduction: Calcium-aluminum-rich inclusions (CAIs) are significant objects occurring within chondritic meteorites. Based on radiometric dating and thermodynamic modelling they are considered to be some of the first solids to condense from a cooling gas of solar composition [1-4]. Therefore, they provide a window into the early solar system's chemistry.

Many CAIs are surrounded by multi-layered, thin mineral sequences, called Wark-Lovering Rims (WLR)[5]. Different formation mechanisms have been discussed for these rims, among them condensation, metasomatic exchange and flash heating [6-11].

The electron and ion microprobes have been extensively used to study CAIs [12-14]. Information on the three-dimensional structure of CAIs, such as that offered by FIB tomography [15-18], could provide new insights into their origins. Initial work demonstrated the potential of FIB tomography toward understanding CAI origins [19] however, detailed method development for planetary materials has not to our knowledge been performed. Here, we present 3D reconstruction of the internal structure of different locations of WLR from a CAI within the Allende meteorite.

Material & Methods: We studied a CAI in a section of the Allende CV3 chondrite, from the University of Arizona collection (UoA 28-4). The Cameca SX-100 electron microprobe (EMP) at the Kuiper Materials Imaging and Characterization Facility (KMICF) at the University of Arizona (https://kmicf.lpl.arizona.edu) were used to obtain backscattered electron (BSE) images to identify a suitable location for FIB tomography. EMP analysis of the CAI rim was done using 1µm beam size at 20nA current and 15kV voltage. The wavelength-dispersive spectrometers were calibrated using well-characterized natural minerals and materials. 3D Tomography datasets and EDS maps were obtained using ThermoFisher Helios 660 G^3 dualbeam FIB equipped with an integrated EDAX EDS detector also at KMICF. Data was analyzed using Avizo 19.2.

Results & Discussion: In this study, we selected a specific region of the WLR surrounding the CAI identified by microprobe analysis (Fig. 1 a+b).

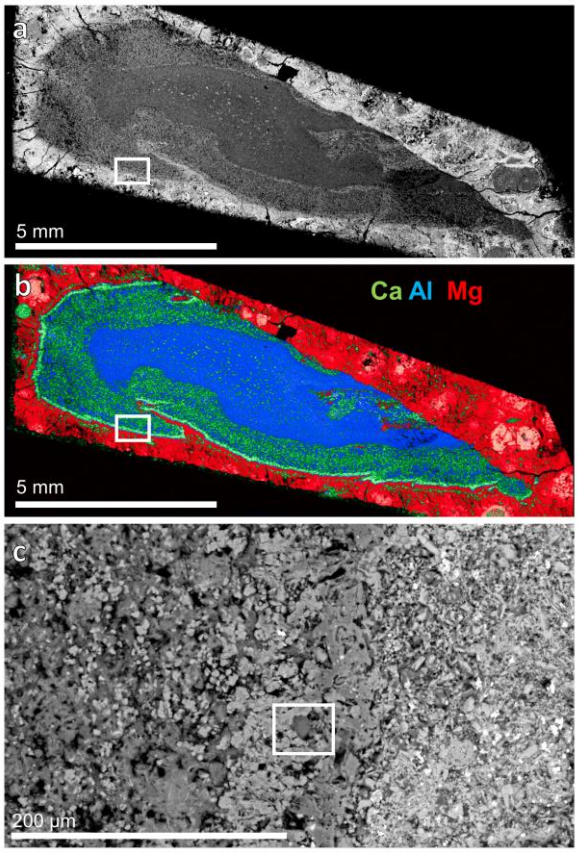

Figure 1. Microprobe and FIB data on the section of the Allende CAI. (a) BSE overview showing region of interest for FIB tomography (white box). (b) False-color WDS map of the section showing Ca (green channel), Al (blue channel) and Mg (red channel). (c) Higher magnification BSE of the ROI in which tomography was performed (white box).

The following mineral phases were identified in this region via WDS spectra analyses: spinel, olivine, nepheline and hibonite. Illustrative stoichiometry includes spinel, $Mg_{0.74}Fe_{0.25}Al_{1.99}O_4$ and olivine, $Mg_{1.22}Fe_{0.76}Si_{0.99}O_4$ and $Mg_{1.2}Fe_{0.79}Si_{0.99}O_4$. To enable the visualization of the interface in FIB tomography, it was oriented perpendicular to the direction of FIB slicing (Fig. 1 c). A total of 247 slices with 20 nm thickness were collected (representative images in Figure 2). A complex microstructure of grain boundaries, macropores and nanopores concentrated along grain boundaries were observed.

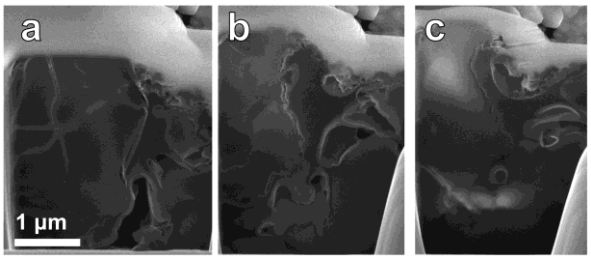

Figure 2. Representative SEM images from FIB tomography slides showing the complex microstructure of the probed WLR.

Summary: In this study, we demonstrate successful FIB tomography characterization of WLR in the KMICF. Further refinement of both measurement conditions and data analyses are required to maximize scientific output of these analyses. We will combine FIB tomography analyses with FIB lift out for transmission electron microscopy sample preparation. The method development demonstrated here will enable the 3D FIB-tomography of samples to be returned from the Hayabusa 2 and OSIRIS-REx missions.

References: [1] Lodders K. Astrophys J. 2003;591(2):1220. [2] Ebel DS. Meteorites early Sol Syst II. 2006;1:253–77. [3] Amelin Y et al. Science (80-). 2002;297(5587):1678–83. [4] Connelly JN et al. Science (80). 2012;338(6107):651–5. [5] Wark DA, Lovering JF. Lunar and Planetary Science Conference Proceedings. 1977. p. 95–112. [6] MacPherson GJ, et al. Lunar and Planetary Science Conference. 1981. p. 648–51. [7] Macpherson GJ, Grossman L. Geochim Cosmochim Acta. 1984;48(1):29–46. [8] Davis AM, et al. Meteoritics. 1986;21:349. [9] Davis AM, MacPherson GJ. Meteoritics. 1994;29:458–9. [10] Wark D, Boynton W V. Meteorit Planet Sci. 2001;36(8):1135–66. [11] Krot AN, et al. Meteoritics. 1995;30(6):748–75. [12] Koike O, et al. Antarct Meteor Res. 1993;6:357. [13] Grossman L. Geochim Cosmochim Acta. 1975;39(4):433–54. [14] Simon SB, et al. Geochim Cosmochim Acta. 1994;58(8):1937–49. [15] Liu S, et al. J Pet Sci Eng. 2017;148:21–31. [16] Zhou S, et al. Int J Coal Geol. 2017;174:41–54. [17] Munroe PR. Mater Charact. 2009;60(1):2–13. [18] Weber J, et al. Chem Geol. 2017;466:722–32. [19] Zega TJ. Microsc Microanal. 2015;21(S3):2105–6.

Acknowledgment:

We acknowledge NASA grants #NNX12AL47G, #NNX15AJ22G and #NNX07AI520, and NSF grants #1531243 and #EAR-0841669 for funding of the instrumentation in the Kuiper Materials Imaging and Characterization Facility at the University of Arizona. Research supported by NASA Emerging Worlds Program (grant # 80NSSC19K0509).